# Doped semiconductors as half-metallic materials: Experiments and first-principles calculations of $CoTi_{1-x}M_xSb$ ($M$=Sc, V, Cr, Mn, Fe)

Benjamin Balke, Gerhard H. Fecher, Andrei Gloskovskii, Joachim Barth, Kristian Kroth, and Claudia Felser*
*Institut für Anorganische und Analytische Chemie, Johannes Gutenberg-Universität, D-55099 Mainz, Germany*

Rosa Robert and Anke Weidenkaff
*EMPA, Swiss Federal Laboratories for Materials Testing and Research, Solid State Chemistry and Catalysis, CH-8600 Duebendorf, Switzerland*

(Received 10 July 2007; revised manuscript received 15 October 2007; published 23 January 2008)

This work reports experiments and first-principles calculations on the substitutional semiconducting $C1_b$ compound $CoTi_{1-x}M_xSb$. Diluted magnetic semiconductors have been prepared by substituting titanium in the semiconducting compound CoTiSb by other 3*d* transition elements *M*. Self-consistent calculations of the electronic structure predict some of the materials to be half-metallic ferromagnets. The structural, electronic, electric, and magnetic properties of the pure and substituted materials have been investigated. It is found from the experiments that substitution of up to 10% Ti by Fe, Mn, Cr, and V does not affect the crystalline structure and the lattice mismatch is less than 0.5% in the substituted compounds. The electric properties can be tuned from semiconducting to metallic by using different dopants. The $M$=Cr-doped compound exhibits a metal to semiconductor transition. Photoemission spectroscopy and conductivity measurements agree well with the calculated electronic structure. The measured Curie temperature of the Fe-substituted alloy is far above room temperature (>700 K). This fact and the very low lattice mismatch between the substituted and the pure compound make this material a serious candidate for future electronic applications, in particular for magnetoelectronics and spintronics.

DOI: 10.1103/PhysRevB.77.045209 PACS number(s): 75.50.Pp, 72.80.Ga, 71.20.Be, 61.05.cp

## I. INTRODUCTION

Over the last 40 years, the semiconductor industry has been able to continually shrink the size of electronic components on silicon chips, packing ever more performance into computers. The limits of the current technology are reached, when smaller component sizes are prevented by the fundamental physical laws. In the last decade, spintronics has been developed as a new approach that has revolutionized the market for electronic devices. Some predicted advantages of this new technology are the nonvolatility of data storage, the increased speed of data processing, the high storage density, and the low energy consumption. To exploit the full potential of spintronics, the development of new magnetic materials, magnetic semiconductors, and half-metallic ferromagnets (HMFs) is necessary.[1] Half-metallic ferromagnets meet all the requirements of spintronics, as a result of their exceptional electronic structure. These materials behave like metals with respect to the electrons of one spin direction and like semiconductors with respect to the electrons of the other spin direction.

Many attempts have been made to prepare semiconducting compounds that also have ferromagnetic properties. Mn-doped GaAs (Ref. 2) was considered to be a suitable compound, but its Curie temperature is only about 150 K (Ref. 3) and thus still far away from being suitable for application in electronic devices (see Ref. 4 for a recent review). Other materials, such as Mn-doped GaN ($T_C$=228 to 370 K),[5] V-doped $TiO_2$ ($T_C \approx 400$ K),[6] *p*-(Ga,Ni)N ($T_C \approx 300$ K),[7] $NiTi_{0.9}Mn_{0.1}Sn$ ($T_C \approx 330$ K),[8] or Co-doped ZnO ($T_C > 300$ K),[9] come only close to room temperature or need special treatments.

The $C1_b$ compound NiMnSb was one of the early materials being predicted to be a HMF by electronic structure calculations.[10] Two alternative structural descriptions of the $C1_b$ structure (space group $F\bar{4}3m$) are possible. The common description is that the $C1_b$ compounds of composition *XMZ* (*X*, *M*=transition metals, *Z*=main group element) consist of three interpenetrating FCC lattices. From the viewpoint of electronic structures, the most appropriate description of these compounds is a zinc-blende *MZ* lattice stuffed with *X* atoms (see Fig. 1).

In 1984, Kübler found that the Slater-Pauling rule is useful for describing the magnetic properties of $C1_b$ compounds.[11] Jung *et al.*[12] recognized that many *XMZ* compounds can be thought of as comprising $X^{n+}$ ions stuffed in a

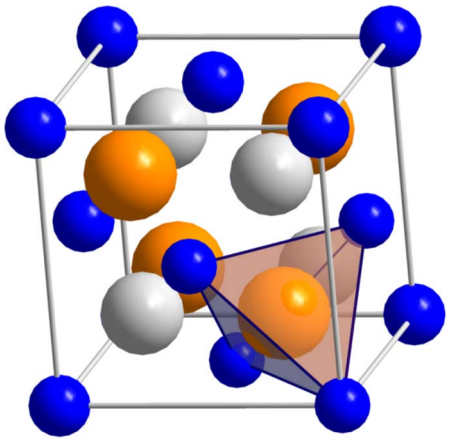

FIG. 1. (Color online) Crystal structure of $CoTi_{1-x}M_xSb$. The Ti (or *M*) atoms are placed in the centers of tetrahedra formed by Co.

 

zinc-blende-type $[MZ]^{n-}$ sublattice, where the number of valence electrons associated with the $[MZ]^{n-}$ sublattice is 18 $(d^{10}+s^2+p^6)$. Such closed-shell 18-electron compounds are nonmagnetic and semiconducting.[13–15] The prototype for a nonferromagnetic compound is CoTiSb. This compound is, among other $C1_b$ compounds, often used as a base for thermoelectric materials[16,17] by substitution of Ti by other transition metals[18] or by substituting Sb by Sn.[19]

On the other hand, most of the magnetic and half-metallic $C1_b$ compounds contain manganese or a rare earth metal. This is not accidental because the properties of the manganese ions in the $M$ position of the $C1_b$ compounds must be taken into account, as described by Kübler *et al.*[20] These manganese ions, which have an approximate $Mn^{3+}$ configuration, exhibit a highly localized moment in the order of $3-4\mu_B$. The rare earth (RE) ions in $C1_b$ compounds (for example, RENiSb or REAuSn) also exhibit a charge of +3 and a magnetic moment corresponding to localized $f$ states.[21] It is expected that substitution of one of the 3$d$ metals in the 18-electron compounds leads to the formation of localized magnetic moments. The electronic and magnetic structures of various dilute magnetic semiconductors based on $C1_b$ compounds were calculated by Nanda and Dasgupta[22] or more recently by Fukushima *et al.*[23]

The present work focuses on the search of suitable compounds that bridge both semiconducting and ferromagnetic properties in almost one material. Therefore, Ti 3$d$ transition metal substituted compounds based on the semiconducting CoTiSb were prepared and investigated both theoretically and experimentally.

## II. COMPUTATIONAL DETAILS

The electronic structure has been calculated for pure and Ti-$M$ substituted $CoTi_{1-x}M_xSb$ (where $M$=Sc, V, Cr, Mn, Fe) in order to examine their electronic and magnetic properties. Self-consistent calculations have been performed by means of the full-relativistic, spin polarized Korringa-Kohn-Rostocker (KKR) method in combination with the coherent potential approximation (CPA).[24,25] CPA allows electronic structure calculations for systems with random distribution of the atoms as is here the case where $M$ substitutes partially for Ti.

For the ordered substitutional compounds, the CPA method has been used to model the statistic distribution of the atoms on the $M$ site and the Ti atoms on a common site of the $C1_b$ crystalline structure. The Co atoms are placed on the 4$a$ Wyckoff position, the Ti atoms are placed together with the atoms on the $M$ site on the 4$c$ position, and the main group element Sb is finally placed on the 4$d$ position of the cell with $F\bar{4}3m$ symmetry. The disordered CoTiSb compound also has been treated using the CPA method by placing vacancies on regular sites and simultaneously the swapped or excessed part on the 4$b$ Wyckoff position. Six different kinds of disorder have been respected, as summarized in Table I.

The calculations have been performed using one of the most common parametrizations of the exchange-correlation functional as given by Vosco *et al.*[26–28] Additionally, the generalized gradient approximation has been used in the form given by Perdew *et al.*[29] The CPA tolerance has been set to $10^{-4}$ and the energy convergence criterion to $10^{-5}$. $f$ states are included in the basis of all atoms, as it turned out that $l=2$ is a too small value for the orbital momentum to explain the magnetic properties correctly. 578 irreducible $k$ points based on a $22\times22\times22$ mesh have been used for integration. The density of states is calculated for the same number of $k$ points from the Green function by adding a small imaginary part of 2 mRy to the energy. For smaller values, the band gaps may become better visible; however, at the same time, the DOS becomes much more noisy.

TABLE I. Models for disordered CoTiSb. Given are the site occupation numbers for the four different Wyckoff positions in the $F\bar{4}3m$ lattice. Rows 1–3 give the swapped structures and rows 4–6 the excess or lack structures. The occupancy of the positions by the vacancy (□) is always chosen such that the sum of the occupancies is 1.

| | 4$a$ | 4$b$ | 4$c$ | 4$d$ |
|---|---|---|---|---|
| Co-Vc | 0.9 Co | 0.1 Co | Ti | Sb |
| Ti-Vc | Co | 0.1 Ti | 0.9 Ti | Sb |
| Sb-Vc | Co | 0.1 Sb | Ti | 0.9 Sb |
| Co excess | Co | 0.05 Co | Ti | Sb |
| TiSb lack | Co | □ | 0.95 Ti | 0.95 Sb |
| Excess/lack | Co | 0.05 Co | 0.95 Ti | 0.95 Sb |

Partial cross sections have been calculated for better comparison of the calculated electronic structure with the valence band photoemission spectra. The orbital momentum and site resolved cross sections were calculated for atomic valence states using a modified fully relativistic Dirac solver based on the computer programs of Salvat and Mayol.[30,31] The radial integrals for the various transitions ($s\rightarrow p$, $p\rightarrow s,d$, and $d\rightarrow p,f$) have been computed using the dipole length form. In addition, the electron mean free path was calculated using the Tanuma-Powell-Penn (TPP-2M) equations.[32]

## III. EXPERIMENTAL DETAILS

$CoTi_{1-x}M_xSb$ ($M$=V, Cr, Mn, Fe) samples have been prepared by arc melting of stoichiometric amounts of the constituents in an argon atmosphere at $10^{-4}$ mbar. Special care was taken to avoid oxygen contamination. This was ensured by evaporating Ti inside the vacuum chamber before melting the compound as well as by additional purifying of the process gas. The resulting polycrystalline ingots were afterward annealed in evacuated quartz tubes for 14 days at 1073 K. This procedure resulted in samples exhibiting the $C1_b$ structure. Flat disks were cut from the ingots and polished for spectroscopic investigations of bulk samples. For powder investigations, the remainder was crushed by hand using a mortar. The correct structure has been verified by x-ray powder diffraction (XRD) using excitation by Cu $K\alpha$ radiation.

The temperature dependent XRD measurements have been performed at the x-ray powder diffraction beamline at

the bending magnet D10 at the Brazilian Synchrotron Light Laboratory (LNLS). For details about the characteristics of the beamline, see, e.g., Ref. 33. The temperature was varied from 20 to 300 K using a closed cycle cryostat and resistive heating. The excitation energy was set to $h\nu=7050$ eV corresponding to a photon wavelength $\lambda=1.758\,86$ Å.

X-ray photoemission spectroscopy (XPS) was used to verify the composition and to check the cleanliness of the samples. After removal of the native oxide from the polished surfaces by $Ar^+$ ion bombardment, no impurities were detected with XPS. When exposed to air after the basic cleaning, the samples exhibited a thin (<1 nm) layer of oxidized Sb at the surface. Therefore, the samples were capped after cleaning *in situ* by a 1–2 nm layer of Au to prevent oxidation of the samples during transport in air.

The magnetic properties have been investigated by a superconducting quantum interference device (SQUID) (Quantum Design MPMS-XL-5) using nearly punctual pieces of approximately 5–10 mg of the sample. The electrical transport property measurements have been carried out on bar shaped pellets ($2\times3\times5$ mm$^3$) of the annealed samples. The electrical resistivity was measured using a Quantum Design Physical Property Measurement System by the four-contact method with silver contacts.

Details of the electronic structure have been explored experimentally by means of photoemission spectroscopy. The hard x-ray photoemission spectroscopy (HAXPES) measurements have been performed at the KMC-1 beamline of the storage ring BESSY (Berlin, Germany). The photons are produced by means of a bending magnet. The photon beam is focused by a toroidal mirror and monochromatized by a double-crystal monochromator. In the present work, Si(111) crystal pairs have been used which can be employed for photon energies up to ≈15 keV with a starting energy of 1.997 keV, however, with rapidly decreasing resolution. The spot size of the beam is $(0.4\times0.6)$ mm$^2$ at the sample. The complete beamline is operated under oil-free UHV conditions ($<5\times10^{-8}$ mbar at last valve). For details about the characteristics of the beamline, see Ref. 34.

As electron analyzer, a recently developed hemispherical spectrometer with 225 mm radius has been used (SPECS PHOIBOS 225 HV). The analyzer is designed for high resolution spectroscopy at kinetic energies up to 15 keV. The analyzer is equipped for parallel (energy and angle) detection using a two-dimensional (2D)-delay-line detector. For the present study using relatively high kinetic energies, the 2D detector has been employed for energy detection only. Typical spectra, as taken from a Au(100) single crystal, were reported in Ref. 34.

Under the present experimental conditions, an overall resolution of 240 meV at 2 keV photon energy has been reached (monochromator plus electron detector), as was determined from the Fermi edge of Au(100). Due to the low cross section of the valence states from the investigated compounds, the spectra had to be taken with $E_{pass}$ from 50 to 150 eV and a 1 mm entrance slit for a good signal to noise ratio.

The soft x-ray photoemission spectroscopy measurements have been performed at the UE52-SGM undulator beamline (former U49) of BESSY using the PHOIBOS 225 HV spectrometer. The beamline provides soft x-ray radiation in the energy range from 100 to 1600 eV. For the present measurements, the exit slit was set to 100 $\mu$m for a nominal resolution of about $10^4$ at 750 eV for the grating with 1200 lines/mm resulting in an energy resolution of better than 100 meV. For details about the characteristics of the beamline—flux and resolution—see Ref. 35.

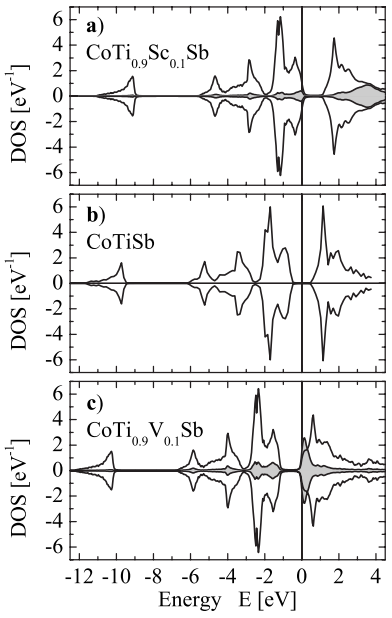


FIG. 2. Spin resolved density of states of (a) $CoTi_{0.9}Sc_{0.1}Sb$, (b) CoTiSb, and (c) $CoTi_{0.9}V_{0.1}Sb$. The additional DOS arising from the $M$ site (shaded areas) is multiplied by a factor of 5 for better visibility.

The photoemission spectra reported below were obtained from samples cleaned by $Ar^+$ ion bombardment just before the measurements. All photoemission spectra were taken at room temperature.

## IV. RESULTS: FIRST-PRINCIPLES CALCULATIONS OF THE ELECTRONIC STRUCTURE

The electronic structure has been calculated for pure and substituted $CoTi_{0.9}M_{0.1}Sb$ ($M$=Sc,V,Cr,Mn,Fe) using the full-relativistic, spin polarized KKR method in combination with the CPA. The calculated densities of states (DOSs) are shown in Figs. 2 and 3. For a better comparison, the minority states are shown on a negative scale. As predicted by Tobola and Pierre,[36] CoTiSb is a semiconductor with a gap at the Fermi energy for both spin directions. All calculated densities show principally the same structure. The low lying $s$ states are found at about 11–9 eV below the Fermi energy and are separated from the high lying $d$ states by the $C1_b$-typical hybridization gap. The size of this gap amounts typically to $\Delta E\approx3,\ldots,4$ eV in Sb containing compounds. It indicates the strong covalent bonding between the Ti atoms or the atoms on the $M$ site and the Sb atoms.

While the calculations for $CoTi_{0.9}Sc_{0.1}Sb$ and $CoTi_{0.9}V_{0.1}Sb$ result in nearly semiconducting behavior, the calculations show a half-metallic behavior for

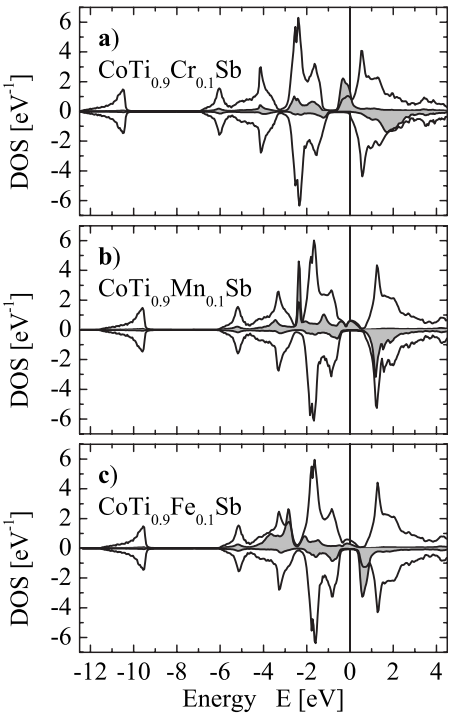


FIG. 3. Spin resolved density of states of (a) $CoTi_{0.9}Cr_{0.1}Sb$, (b) $CoTi_{0.9}Mn_{0.1}Sb$, and (c) $CoTi_{0.9}Fe_{0.1}Sb$. The additional DOS arising from the $M$ site (shaded areas) is multiplied by a factor of 5 for better visibility.

$CoTi_{0.9}Cr_{0.1}Sb$, $CoTi_{0.9}Mn_{0.1}Sb$, and $CoTi_{0.9}Fe_{0.1}Sb$. Figure 2 compares the spin resolved densities of states of (a) $CoTi_{0.9}Sc_{0.1}Sb$, (b) CoTiSb, and (c) $CoTi_{0.9}V_{0.1}Sb$. For CoTiSb, the Fermi energy ($\epsilon_F$) is set in the middle of the semiconducting gap. In the case of substituting 10% Ti by Sc, the gap shifts with respect to the Fermi energy to the top of the valence band like in $p$-type semiconductors. On the other hand, if 10% Ti is substituted by V, then the gap shifts with respect to the Fermi energy to the bottom of the conduction band, like in $n$-type semiconductors. In the V-substituted compound, the strong localization of the additional $d$ states at the bottom of the conduction band is obvious. In both cases, the occupied states in the valence bands are distributed similar to those in the pure compound.

The situation changes if doping CoTiSb with more $d$ electrons. Partial replacement of titanium by Cr, Mn, or Fe (10%) has the result that the semiconductor is converted into a HMF: the DOS at the Fermi energy is clearly different from zero for only one spin direction, while remaining zero for the other (see Fig. 3). An interesting observation is that the half-metallicity has different reasons in the three different cases. In the $CoTi_{0.9}Cr_{0.1}Sb$ case, the Cr $3d$ states fill up directly the gap at $\epsilon_F$ in the majority channel, similar to the V-substituted compound. In the $CoTi_{0.9}Mn_{0.1}Sb$ case, the localized Mn $3d$ states fill the band gap at approximately 2.5 eV below $\epsilon_F$ in the majority channel. These Mn $3d$ states shift the majority Co states from the valence band into the gap. The situation is similar to the Ti-Mn-substituted NiTiSn, as reported by Sanyal *et al.*[8] The calculation shows a similar result when substituting 10% Ti in CoTiSb by Fe. The main parts of the additional Fe $3d$ states are located at approximately 3 eV below $\epsilon_F$—note that the Fe $3d$ states are not filling up the band gap like the Cr states in $CoTi_{0.9}Cr_{0.1}Sb$—and therefore the Co states are shifted into the majority gap. At the same time, the minority gap is reduced due to unoccupied, additional Fe $d$ states at the bottom of the minority conduction band. In contrast, Cr or Mn substitution does not effect the minority band gap and the additional states are located well above $\epsilon_F$. This results in a clear and stable band gap. The exchange splitting between the occupied and unoccupied localized $d$ states in the Mn- and Fe-substituted compounds amounts to about 3.6 and ≈3.4 eV, respectively.

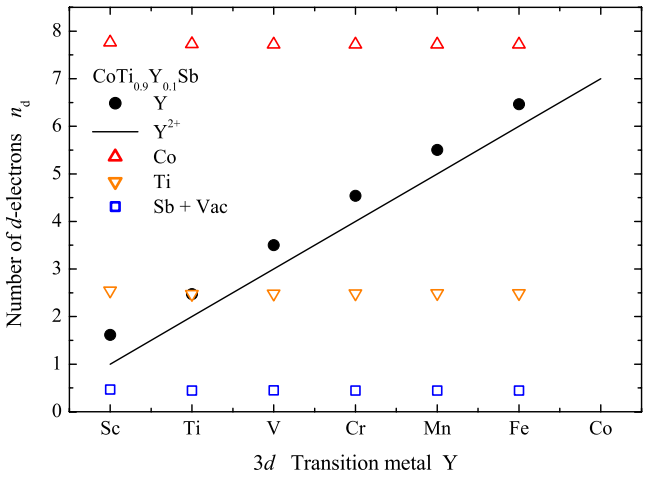


FIG. 4. (Color online) Number of $d$ electrons in $CoTi_{0.9}M_{0.1}Sb$ where $M$=Sc,Ti,V,Cr,Mn,Fe. The full line is the expected value for $M^{2+}$ ions.

A further important result of the calculations is that only the $M$=Cr,Mn,Fe atoms and, moreover, only those atoms on the $M$ site replacing Ti contribute to the total magnetic moment of the compound. The atoms on the $M$ site on Co positions or in vacant tetrahedral holes should not contribute to the magnetic moment at all. This was verified for the $M$=Fe-substituted compound by Mössbauer spectroscopy and x-ray magnetic circular dichroism (XMCD) measurements, as reported in Ref. 37. XMCD revealed that only the Fe atoms carry a magnetic moment. Mössbauer spectroscopy confirmed only a single magnetic hyperfine field and a very small paramagnetic contribution. The latter arises from Fe atoms on one or both of the possible nonmagnetic sites. The calculated value of the magnetic moment per iron atom changes slightly from 3.4 $\mu_B$ (at 5%) to 3.7 $\mu_B$ (at 10%) with increasing Fe concentration on the Ti position.

Figure 4 compares the calculated number of $d$ electrons on the $M$ site to those of the fixed atoms of $CoTi_{0.9}M_{0.1}Sb$ ($M$=Sc,Ti,V,Cr,Mn,Fe). For Co, Ti, and Sb (including the vacant position), the results show no dependence on the number of $d$ electrons on the doping element. On the Co site, there are formally 7.75 $d$ electrons, while there are 2.5 and 0.45 $d$ electrons on the Ti site and the Sb site including the vacancy, respectively. The number of $d$ electrons on the $M$ site increases linearly with the kind of $3d$ transition metal, as expected. There is an excess of approximately 0.5 $d$ electrons compared to the expected value for $M^{2+}$ ions. These results exclude charge-transfer effects and point certainly on local-

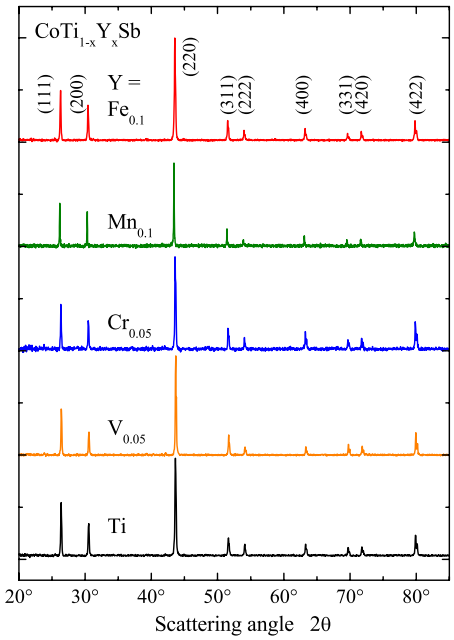


FIG. 5. (Color online) XRD spectra for $CoTi_{1-x}M_xSb$ where $M=Ti,V,Cr,Mn,Fe$. The spectra were excited by Cu $K\alpha$ radiation

ized moments on the $M$ sites. This is obvious, in particular, for Mn [see Fig. 3(b)], where a sharp feature appears in the majority states.

## V. RESULTS AND DISCUSSION

### A. Structural properties

$CoTi_{1-x}M_xSb$ ($M=V,Cr,Mn,Fe$) samples have been prepared and it was carefully proved that the atoms on the $M$ site occupy in majority the Ti positions and not another vacant site. For that purpose, the x-ray powder diffraction patterns of the substituted compounds were compared to those of pure CoTiSb. It was observed that no additional diffraction reflexes appear up to 10% $M$ substitution. This confirms that the structure remains the same as of pure CoTiSb, that is, $C1_b$. The diffraction patterns of pure and 10% Fe and Mn and 5% Cr- and V-substituted samples are compared in Fig. 5. The change of the lattice parameter $a=5.886$ Å for CoTiSb is small ($\approx 0.2\%$) if 10% of Ti is replaced by any of the atoms on the $M$ site as expected due to the similar radii of the $3d$ transition metals. The very small lattice mismatch between pure and substituted compounds is a very important result if thinking about preparing thin film devices combined from pure and substituted materials. It should be possible to grow them epitaxially with clean and smooth interfaces. If depositing layer by layer, one can use the Co planes to merge the different materials without any interface at all.

The $R$ values for the best fits in the Rietveld refinement are $R_i=6\%$ and $R_p=11\%$, confirming the high degree of site order of the samples. It should be noted that the structure was hardly stabilized in the correct $C1_b$ structure for Mn substitution.

The structural parameter of CoTiSb has been investigated in dependence of the temperature between 20 and 300 K.

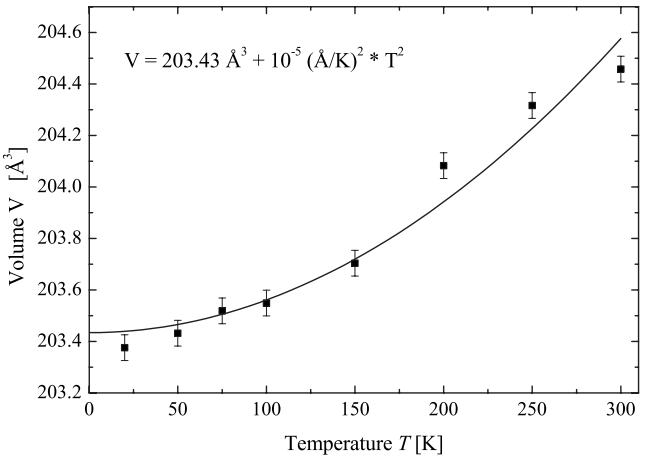


FIG. 6. Temperature dependency of the cubic cell volume $V$ for CoTiSb. The fit of the data to a $T^2$ dependence is shown as a full line.

Figure 6 shows the temperature dependency of the cell volume $V=a^3$ of the cubic cell. The volume decreases by about 0.5% if the temperature is lowered from room temperature to 20 K. The change of the cell volume with temperature is clearly nonlinear and evidence is given that the volume increases with an approximate $T^2$ law.

Further, iron-substituted $CoTi_{0.9}M_{0.1}Sb$ samples have been investigated by means of transmission electron microscopy (TEM) in order to prove the homogeneity of the sample. Uniform TEM images were observed and, in particular, no Fe clusters were detectable. Figure 7 shows a typical diffraction pattern taken at 120 keV exhibiting the cubic structure of the compound.

### B. Magnetic properties

If the $C1_b$ compounds are half-metallic ferromagnets, then their magnetization will show a Slater-Pauling-like behavior.

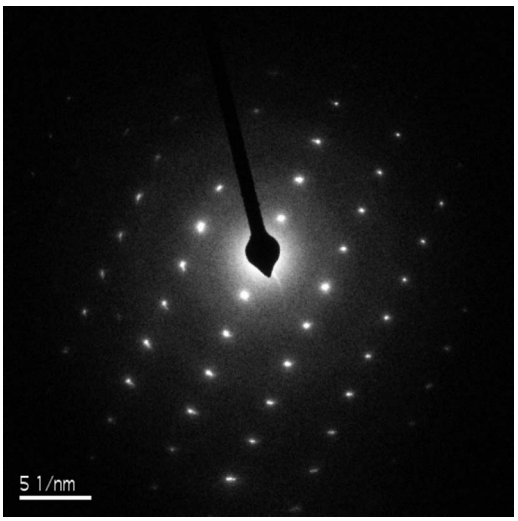


FIG. 7. Transmission electron microscopy image of $CoTi_{0.9}Fe_{0.1}Sb$. The TEM diffraction pattern shows the cubic symmetry of the sample.

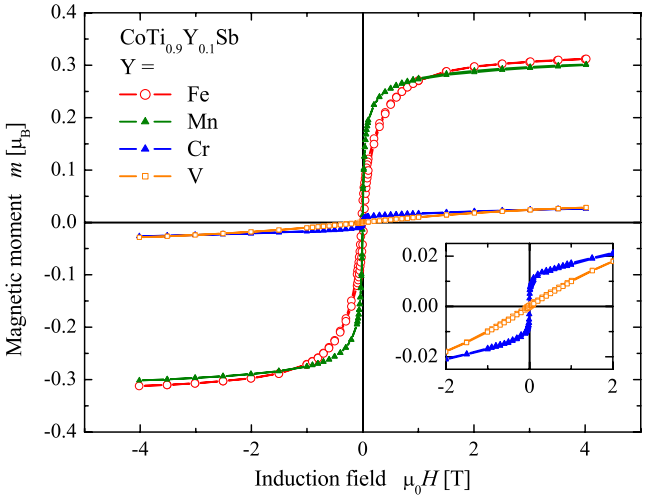


FIG. 8. (Color online) Magnetic moments for $CoTi_{1-x}M_xSb$ where $M$=V, Cr, Mn, Fe. The data for the Cr and V containing samples are shown in the inset on an enlarged scale.

This means that the saturation magnetization scales linearly with the number of valence electrons.[12,38,39] The magnetic moment per unit cell (in multiples of the Bohr magneton $\mu_B$) is given by

$$m = N_V - 18, \tag{1}$$

where $N_V$ is the accumulated number of valence electrons in the unit cell. For CoTiSb, there is a total of 9+4+5=18 valence electrons in the unit cell. This results in no magnetic moment at all.

Low temperature magnetometry has been carried out by means of SQUID to investigate the influence of the dopants on the magnetic properties and to compare the results with the calculated saturation moments. Selected results are shown in Fig. 8.

The total magnetic moments of the ferromagnetic samples, measured at 5 K and in saturation, are 0.32 $\mu_B$, 0.30 $\mu_B$, and 0.02 $\mu_B$ for $CoTi_{0.9}Fe_{0.1}Sb$, $CoTi_{0.9}Mn_{0.1}Sb$, and $CoTi_{0.9}Cr_{0.1}Sb$, respectively. The pure CoTiSb exhibits a diamagnetic behavior, while the V-substituted sample is paramagnetic. Figure 9 displays the dependence of the saturation moment as a function of the atoms on the $M$ site and compares the calculated moments with the experimental results.

The experiments confirm the calculations which result in ferromagnetic samples in the case of $CoTi_{0.9}Fe_{0.1}Sb$, $CoTi_{0.9}Mn_{0.1}Sb$ and $CoTi_{0.9}Cr_{0.1}Sb$ but remain nonmagnetic for $CoTi_{0.9}V_{0.1}Sb$ and $CoTi_{0.9}Sc_{0.1}Sb$. However, the measured magnetic moment of the Cr-substituted compound is much too low compared to the calculation. This might be due to a partial antiferromagnetic order of the Cr moments or by a partial occupation of the vacant site, like observed in the Fe-substituted compound to a very small amount. To determine the Curie temperatures of the compounds, high temperature magnetometry was performed up to 800 K. The Curie temperature of $CoTi_{0.9}Fe_{0.1}Sb$ is above 700 K. However, it cannot be determined more precisely because the onset of decomposition of the alloy was observed at about that temperature (see Ref. 37). This value of $T_C$ is considerably higher compared to below 350 K in $NiTi_{1-x}Mn_xSn$.[8] The magnetic transition of the Cr-substituted compound was found at a temperature of about 60 K. The structure of the Mn-substituted compound was too unstable to determine unambiguously the Curie temperature.

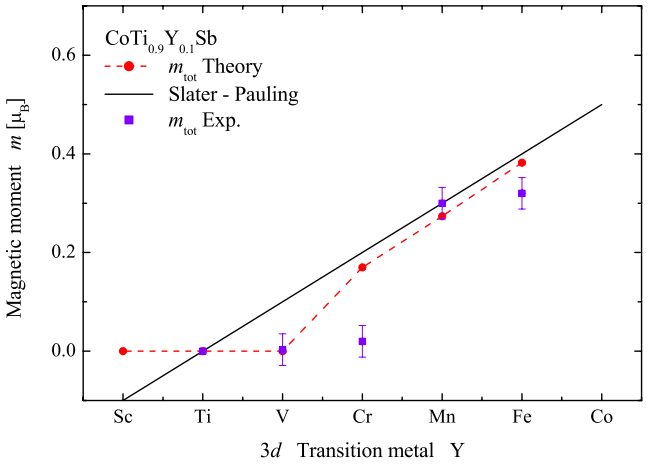


FIG. 9. (Color online) The calculated and measured magnetic moments of $CoTi_{0.9}M_{0.1}Sb$ where $M$=Sc, Ti, V, Cr, Mn, Fe. The Slater-Pauling expected value is shown for comparison.

### C. Electric properties

To prove the predictions from the electronic structure calculations, measurements of the resistivity have been carried out. Figure 10 displays the temperature dependence of the resistivity for pure CoTiSb, $CoTi_{0.95}V_{0.05}Sb$, $CoTi_{0.95}Cr_{0.05}Sb$, and $CoTi_{0.95}Fe_{0.05}Sb$ in the temperature range from 15 to 350 K. The pure CoTiSb and $CoTi_{0.95}V_{0.05}Sb$ show a semiconducting behavior, while $CoTi_{0.95}Fe_{0.05}Sb$ is metallic and $CoTi_{0.95}Cr_{0.05}Sb$ undergoes a metal to semiconductor transition at a transition temperature of $T_t \approx 210$ K.

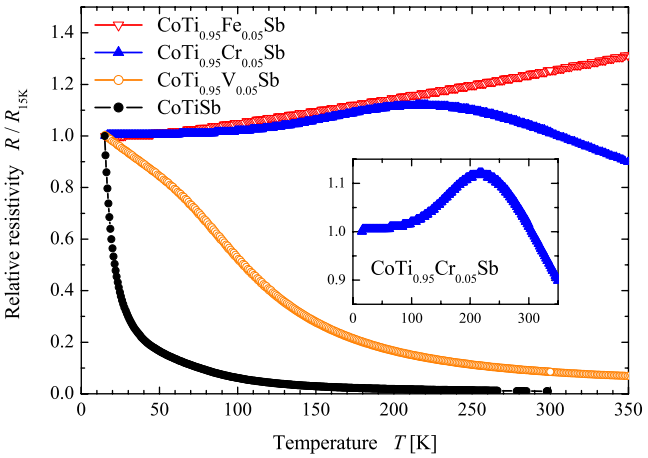


FIG. 10. (Color online) Temperature dependence of the resistivity for CoTiSb, $CoTi_{0.95}V_{0.05}Sb$, $CoTi_{0.95}Cr_{0.05}Sb$, and $CoTi_{0.95}Fe_{0.05}Sb$. The inset shows the result for $CoTi_{0.95}Cr_{0.05}Sb$ on an enlarged scale.

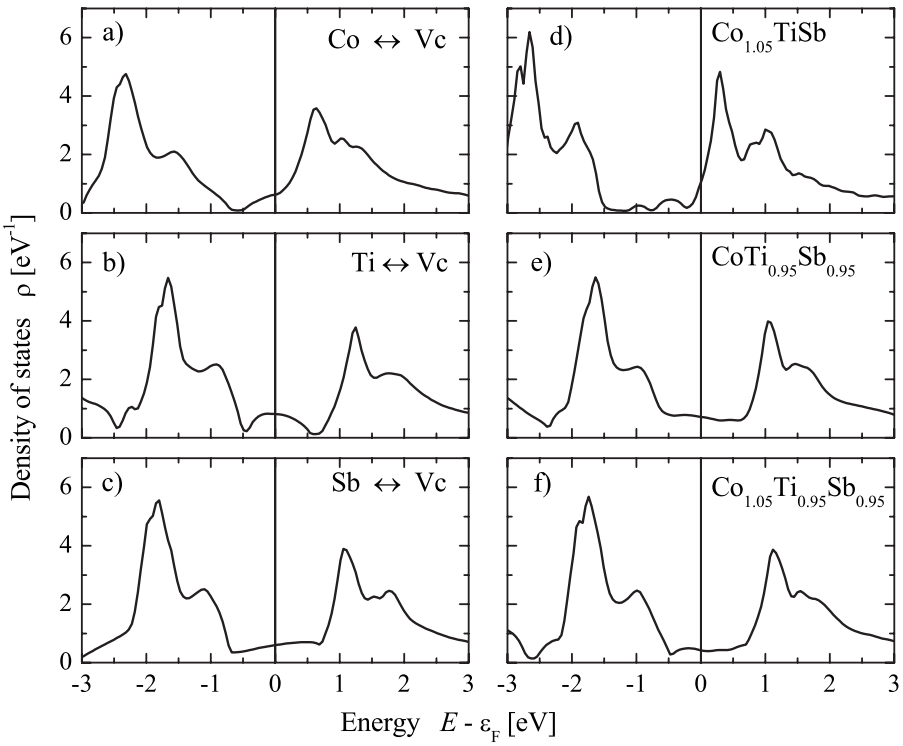


FIG. 11. Density of states for different kinds of disorder of CoTiSb. Panels (a)–(c) show the DOS for the swapped structures and panels (d)–(f) for the excess or lack of structures. The site occupation numbers are given in Table I.

These observations can be explained if considering the number of $d$ electrons being donated by the $M$-Ti substitution in the semiconducting CoTiSb. In the case of replacing 5% titanium by vanadium, there are on average not enough $d$ electrons (doping level 0.05 $e^-$ per cell) to obtain a conducting sample. For 5% iron substitution, there are obviously enough $d$ electrons (doping level 0.2 $e^-$) to end up in a metallic state. In the Cr-substituted sample, one has an intermediate situation. The sample is metallic at low temperature and becomes semiconducting at about $T_t \approx 210$ K.

From the measured temperature dependence of the conductivity of the semiconductors, one can estimate the size of the semiconducting band gap $\Delta E$ from the slope of a $\ln(\sigma)$ vs $(1/T)$ plot making use of

$$\ln(\sigma) = c - \frac{\Delta E}{2k_B}\frac{1}{T}. \tag{2}$$

Here, $\sigma$ is the conductivity, $k_B$ is the Boltzmann constant, and $c$ is a normalization factor. The estimate from the CoTiSb data results in a size of the band gap of $\Delta E \approx 9$ meV. This value is the same, as reported recently by Stadynk *et al.*[40] It is, however, far below the expected value from the electronic structure calculations, even if accounting that the estimation by Eq. (2) is rather rough. In the same way, for $CoTi_{0.95}V_{0.05}Sb$, a very small band gap of $\Delta E \approx 3$ meV is estimated from the data shown in Fig. 10.

One possibility of the small size of the gap might be the occurrence of structural defects being related to the vacancy of one of the positions in the unit cell. The electronic structure was recalculated assuming different kinds of disorder to explain the discrepancy between the calculated gap with a size of $\approx 1$ eV and the one obtained from the resistivity measurements. Six different kinds of disorder have been respected, as summarized in Table I. To avoid numerical instabilities, a disorder level of 5% was used. Figure 11 shows the results of those calculations. The gap is completely smeared out which would result in the metallic behavior of the sample when assuming disorder between Ti [Fig. 11(b)] or Sb [Fig. 11(c)] and the vacancy position or lack of Ti and Sb [Figs. 11(e) and 11(f)]. It is interesting to note that the semiconducting behavior is already destroyed without bringing additional electrons into the system. This means that the semiconducting state relies strongly on the correct $C1_b$ structure.

In the case of assuming disorder between Co and the vacancy position [Fig. 11(a)] or an excess of Co [Fig. 11(d)], the remaining gap is filled up with states and shifted with respect to the Fermi energy. From these calculations, the most probable type of disorder to explain the small band gap is the excess of Co atoms on the vacancy position. This agrees with the XRD data where this type of disorder is the only possibility to improve slightly the quality of the Rietveld refinement. Assumptions of all other types of disorder lead always to an increase of the $R$ values.

### D. Photoemission spectroscopy

Using photoemission spectroscopy, one obtains information about the occupied electronic states. The dispersion of the bands may be studied by spin and angular resolved ultraviolet photoelectron spectroscopy (UPS). This needs, however, well-ordered surfaces of single crystals. For the interpretation, one has to take into account that usually the kinetic energy of the photoemitted electrons is in a range where the mean free path is only a few angstroms and the method therefore mainly shows electronic bands very close to the surface layer.

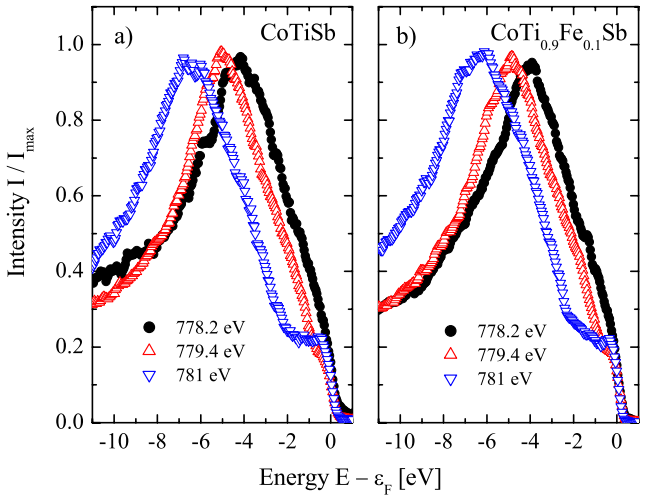


FIG. 12. (Color online) Valence band spectra taken at different excitation energies around the Co $L_3$ edge of (a) CoTiSb and (b) $CoTi_{0.9}Fe_{0.1}Sb$.

Using higher photon energy for excitation (and thus kinetic energies of the photoelectrons), it is possible to study the density of states, in particular, for polycrystalline samples. Making use of resonant excitation, one expects higher bulk sensitivity[41] and may be able to distinguish the site specific contributions. Therefore, both bulk sensitive methods have been applied in the present work.

Figure 12 shows the energy dependence of the valence band photoemission spectra taken with photon energies close to the Co $L_3$ edge for CoTiSb [Fig. 12(a)] and for $CoTi_{0.9}Fe_{0.1}Sb$ [Fig. 12(b)]. The spectra are normalized to the photon flux. The photon energies correspond to the onset of the absorption (778.2 eV), the maximum of the Co $L_3$ white line (779.4 eV), and the trailing edge of the Co $L_3$ absorption (781 eV). For the complete x-ray absorption spectrum, see Ref. 37.

The most prominent feature seen in the spectra is the Co Auger electron emission. The $L_3VV$ Auger electron emission is observed just when the onset of the Co $L_3$ absorption edge is reached. It can be clearly identified from its linear energy dependence (see Fig. 12). On a kinetic energy scale, it stays fixed. Due to the high intensity and the intrinsic width of the Auger transition, it is difficult to observe details of the valence band structure.

Figure 13 compares the valence band spectra of CoTiSb and $CoTi_{0.9}Fe_{0.1}Sb$ in more detail. In panel (a), a slightly higher intensity of the Auger excitation is observed for pure CoTiSb compared to the Fe-substituted sample. It should be noted that the maximum of the Auger transition appears at the same energy (−4.48 eV) for both compounds within ±100 meV. Figure 13(b) shows the spectra of CoTiSb and $CoTi_{0.9}Fe_{0.1}Sb$ close to the Fermi level on a larger scale for a better comparison. The Ag Fermi edge as used for the energy calibration of the spectrometer is shown for comparison (intensity not to scale). Close to the Fermi energy, a slightly higher intensity for the Fe containing sample in comparison with the pure CoTiSb is observed. This behavior is compatible with the electronic structure calculations which predict a higher density close to the Fermi level for $CoTi_{0.9}Fe_{0.1}Sb$. Indeed, the valence band spectra hint on a metalliclike characteristic for both samples. If present, a semiconducting gap with a width of below 100 meV cannot be excluded. Antimony is a well-known surfactant; therefore, the metalliclike character may also be explained by a few monolayer thick conducting Sb layer on top of the surface. The occurrence of a very narrow gap is, however, in agreement with the conductivity measurements (see Sec. V C).

Due to the high intense Auger transition governing the spectrum, an additional analysis is needed. In Ref. 34, it was shown that XPS using Mg $K\alpha$ laboratory sources is not able to explain details of the density of states correctly. Therefore, hard x-ray photoemission spectroscopy with high bulk sensitivity has been performed. Due to the resolution restrictions of the beamline, a photon energy of 2.5 keV was chosen. In that case, the electron inelastic mean free path is expected from the TPP-2M equation[32] to be 3.7 nm in good agreement to the *universal* curve.[42,43] The escape depth corresponds to about 6 cubic cells or 24 metallic monolayers (note that 36%

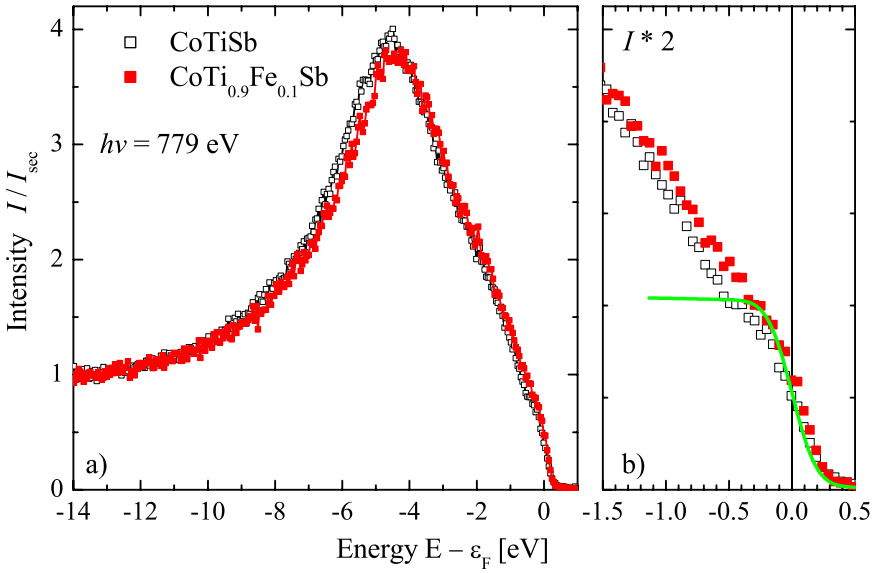


FIG. 13. (Color online) Valence band spectra of CoTiSb and $CoTi_{0.9}Fe_{0.1}Sb$ at 779 eV excitation energy. Panel (a) shows the complete spectra, while panel (b) shows an enlarged view of the area around the Fermi energy. The fitted Ag Fermi edge (full line) is shown on an enlarged intensity scale for comparison.

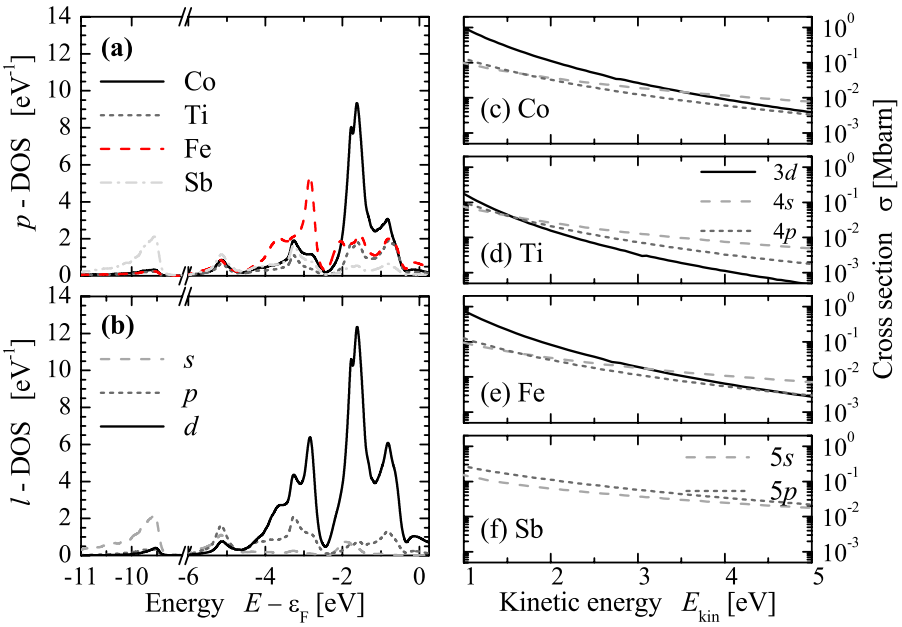


FIG. 14. (Color online) Partial and orbital resolved densities of states and photoemission cross sections. (a) shows the atomic resolved $p$-DOS and (b) shows the orbital momentum resolved $l$-DOS. (Note the axis break between −9 and −6 eV that was used to bridge the low lying hybridization gap.) Panels (c)–(f) show the calculated energy and $l$ dependence of the cross section of the valence states of atomic Co, Ti, Fe, and Sb.

of the intensity emerges still from deeper lying regions of the sample). This value is about 2.5 times higher compared to the resonant excitation at the Co edge.

One further advantage of HAXPES is that the photon energy is in the range where the partial cross sections of the valence states are similar. This avoids an overestimation of emission from $d$ states. To explain that effect, the partial ($p$), atomic resolved, and the orbital ($l$) resolved densities of states for $CoTi_{0.9}Fe_{0.1}Sb$ and the energy and $l$ dependence of the cross section of the valence states of atomic Co, Ti, Fe, and Sb were calculated to compare the measurements and calculations. The orbital momentum and site resolved cross sections are displayed in Figs. 14(c)–14(f). In particular, the cross section for $d$ states decreases faster with increasing photon energy than the ones of the $s$ or $p$ states. This trend is well known.[44] Small differences to the previously published values of Yeh and Lindau[44] are due to the full-relativistic method that was used here to calculate the cross sections.

The partial ($p$) and the orbital ($l$) resolved densities of states for $CoTi_{0.9}Fe_{0.1}Sb$ are shown in Figs. 14(a) and 14(b). The $p$-DOS of the vacancy as well as the $l$-DOS for higher angular momenta ($l$) are omitted as they contribute only very few to the total density of states. The main contributions to states close to the Fermi energy are $d$ states being located at the Co site. The peak in the density at about 3 eV below $\epsilon_F$ is due to the contribution of the Fe $3d$ states. The smaller peak at about −5 eV is due to $s$-$p$ hybridization.

The high energy spectra of CoTiSb and $CoTi_{0.9}Fe_{0.1}Sb$ are shown in Fig. 15. The spectrum calculated by a convolution of the partial and orbital resolved densities with the affiliated cross sections and a Fermi-Dirac distribution is shown for comparison together with the Fe contribution to the spectrum.

Both measured high energy spectra reveal clearly the low lying $s$ states at about 11–9 eV below the Fermi energy, in well agreement to the calculated DOS, see Fig. 15. These low lying bands are separated from the high lying $d$ states by the $C1_b$-typical hybridization gap being clearly resolved in the spectra as well as the calculated DOS. The size of this gap amounts typically to $\Delta E \approx 3, \ldots, 4$ eV in Sb containing compounds.

The structure of the high energy spectra in the range of the $d$ states agrees roughly with the structures observed in the total DOS, although the high density at −5 and −3 eV is not well resolved. Overall, the emission from the $d$ states covers a larger energy range compared to the calculated DOS, which gives advice on an underestimation of correlation effects in the local density approximation. However, one also has to account for lifetime broadening and the experimental resolution if comparing that energy range. At 2.5 keV excitation energy, the emission is still dominated by the high dense $d$ states at about −1.5 eV.

The major difference in the measured valence band spectra between the pure CoTiSb and the Fe-substituted samples

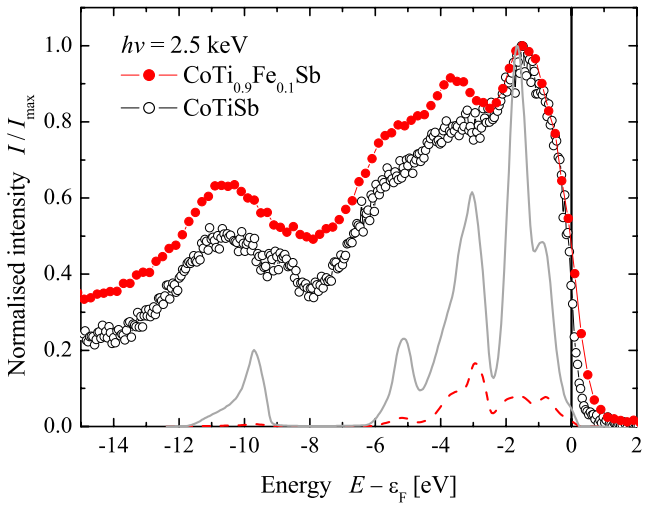


FIG. 15. (Color online) High energy valence band spectra of CoTiSb and $CoTi_{0.9}Fe_{0.1}Sb$. Spectra taken at 2.5 keV excitation energy (symbols) and the DOS of $CoTi_{0.9}Fe_{0.1}Sb$ weighted by the photoemission cross section (lines) are shown. The additional DOS arising from the Fe atom is shown as a dashed line.

is obviously the additional peak at about 3 eV below the Fermi energy. This peak can only be explained with the occurrence of additional Fe 3*d* states in this region of the valence band. They show up in Fig. 14(a) and as well in Fig. 15. A semiconducting band gap of CoTiSb within a width of 100 meV cannot be detected at the given energy resolution of the spectra. The general shape of the high energy photoemission spectra agrees, however, very well with the calculated electronic structure.

## VI. SUMMARY AND CONCLUSION

The $C1_b$ compounds $CoTi_{1-x}M_xSb$ ($M$=Sc,Ti,V,Cr,Mn,Fe) have been synthesized and investigated both experimentally and theoretically. The band structure calculations predict for $CoTi_{0.9}Sc_{0.1}Sb$ and $CoTi_{0.9}V_{0.1}Sb$ a semiconducting behavior as well as a half-metallic behavior for $CoTi_{0.9}Cr_{0.1}Sb$, $CoTi_{0.9}Mn_{0.1}Sb$, and $CoTi_{0.9}Fe_{0.1}Sb$. The measurements of the electric resistivity approve these predictions. The pure CoTiSb and the V-substituted $CoTi_{0.95}V_{0.05}Sb$ compounds exhibit a semiconducting behavior, while $CoTi_{0.95}Fe_{0.05}Sb$ is metallic and $CoTi_{0.95}Cr_{0.05}Sb$ undergoes a metal to semiconductor transition with a transition temperature of $T_t \approx 210$ K. It was shown, however, that any site disorder is able to destroy the semiconducting properties of the parent compound. The calculated magnetic properties agree, in particular, for the Fe- and Mn-substituted compounds, well with the measured properties.

The electronic structure of the CoTiSb and $CoTi_{0.9}Fe_{0.1}Sb$ has been investigated by means of photoemission spectroscopy. In particular, the HAXPES spectra agree with the calculated density of states and show clearly the differences between the pure and the Fe-substituted compound. In particular, the additional Fe 3*d* states were observed at about 3 eV below the Fermi energy. This indicates clearly the localized properties of the doped *d* electrons.

The $C1_b$ structure was verified by XRD for all samples. A very low lattice mismatch is observed between pure CoTiSb and the Ti-$M$-substituted compounds. This result makes that substitutional series interesting for spintronic applications such as spin light emitting diodes or other spin injection devices. One should be able to prepare thin film devices including these materials and it should be possible to grow them epitaxially with clean and smooth interfaces. If depositing layer by layer, one can use the Co planes to merge the different materials without any interface at all.

## ACKNOWLEDGMENTS

The authors thank the staff of BESSY (Berlin) and SPECS (Berlin) for their help during the measurements, L. Gorgeshvili (Mainz) for taking the TEM image, and F. F. Ferreira (LNLS, Campinas) for help with the XRD experiments. The authors are very grateful to H. Ebert (Munich) and his group for developing and providing the SPRKKR computer code. Financial support by DAAD (D06/33952) and CAPES PROBRAL (167/04) is gratefully acknowledged. Further support of this work was provided by the Brazilian Synchrotron Light Laboratory (LNLS) under Proposal No. D10A-XRD2-5708. Part of this work is financially supported by the *Materialwissenschaftliches Forschungszentrum* (MWFZ) of the Johannes Gutenberg-University, Mainz, by BESSY (BMBF 05 ES3XBA/5), and by the Federal Ministry of Education and Research (BMBF 05KS7UMI).

*felser@uni-mainz.de

[1] C. Felser, G. H. Fecher, and B. Balke, Angew. Chem., Int. Ed. **46**, 668 (2007).
[2] H. Ohno, A. Shen, F. Matsukura, A. Oiwa, A. Endo, S. Katsumoto, and Y. Iye, Appl. Phys. Lett. **69**, 363 (1996).
[3] K. W. Edmonds, K. Y. Wang, R. P. Campion, A. C. Neumann, N. R. S. Farley, B. L. Gallagher, and C. T. Foxon, Appl. Phys. Lett. **81**, 4991 (2002).
[4] A. H. MacDonald, P. Schiffer, and N. Samarth, Nat. Mater. **4**, 195 (2005).
[5] M. L. Reed, N. A. El-Masry, H. H. Stadelmaier, M. K. Ritums, M. J. Reed, C. A. Parker, J. C. Roberts, and S. M. Bedair, Appl. Phys. Lett. **79**, 3473 (2001).
[6] N. H. Hong, J. Sakai, and A. Hassini, Appl. Phys. Lett. **84**, 2602 (2004).
[7] R.-T. Huang, C.-F. Hsu, J.-J. Kai, and F.-R. Chen, Appl. Phys. Lett. **87**, 202507 (2005).
[8] B. Sanyal, O. Eriksson, K. G. Suresh, I. Dasgupta, A. K. Nigam, and P. Nordblad, Appl. Phys. Lett. **89**, 212502 (2006).
[9] X. Wang, J. B. Xu, N. Ke, J. Yu, J. Wang, Q. Li, H. C. Ong, and R. Zhang, Appl. Phys. Lett. **88**, 223108 (2006).
[10] R. A. de Groot, F. M. Mueller, P. G. Engen, and K. H. J. Buschow, Phys. Rev. Lett. **50**, 2024 (1983).
[11] J. Kübler, Physica B & C **127**, 257 (1984).
[12] D. Jung, H. J. Koo, and M. H. Whangbo, J. Mol. Struct.: THEOCHEM **527**, 113 (2000).
[13] J. Pierre, R. V. Skolozdra, Y. K. Gorelenko, and M. A. Kouacou, J. Magn. Magn. Mater. **134**, 95 (1994).
[14] J. Tobola, J. Pierre, S. Kaprzyk, R. V. Skolozdra, and M. A. Kouacou, J. Phys.: Condens. Matter **10**, 1013 (1998).
[15] L. Offernes, P. Ravindran, and A. Kjekshus, J. Alloys Compd. **439**, 37 (2007).
[16] Y. Kawahadra, K. Kurosaki, H. Muta, M. Uno, and S. Yamanaka, J. Alloys Compd. **384**, 308 (2004).
[17] T. Sekimoto, K. Kurosaki, H. Muta, and S. Yamanaka, J. Alloys Compd. **394**, 122 (2005).
[18] M. Zhou, L. Chen, C. Feng, D. Wang, and J.-F. Li, J. Appl. Phys. **101**, 113714 (2007).
[19] T. Sekimoto, K. Kurosaki, H. Muta, and S. Yamanaka, J. Alloys Compd. **407**, 326 (2006).
[20] J. Kübler, A. R. Williams, and C. B. Sommers, Phys. Rev. B **28**, 1745 (1983).
[21] H. C. Kandpal, C. Felser, and R. Seshadri, J. Phys. D **39**, 776 (2006).
[22] B. R. K. Nanda and I. Dasgupta, J. Phys.: Condens. Matter **17**, 5037 (2005).

[23] T. Fukushima, K. Sato, H. Katayama-Yoshida, and P. H. Dederichs, J. Phys. Soc. Jpn. **76**, 094713 (2007).
[24] H. Ebert, in *Lecture Notes in Physics*, edited by H. Dreysse (Springer, New York, 1999), Vol. 535, pp. 191–246.
[25] H. Ebert, The Munich SPR-KKR package, Version 3.6, 2005 (http://olymp.cup.uni-muenchen.de/ak/ebert/SPRKKR).
[26] L. Wilk and S. H. Vosko, Phys. Rev. A **15**, 1839 (1977).
[27] S. H. Vosko, L. Wilk, and M. Nusair, Can. J. Phys. **58**, 1200 (1980).
[28] S. H. Vosko and L. Wilk, Phys. Rev. B **22**, 3812 (1980).
[29] J. P. Perdew, K. Burke, and M. Ernzerhof, Phys. Rev. Lett. **77**, 3865 (1996).
[30] F. Salvat and R. Mayol, Comput. Phys. Commun. **62**, 65 (1991).
[31] F. Salvat and R. Mayol, Comput. Phys. Commun. **74**, 358 (1993).
[32] S. Tanuma, C. J. Powell, and D. R. Penn, Surf. Interface Anal. **21**, 165 (1993).
[33] F. F. Ferreira, E. Granado, W. Carvalho, Jr., S. K. S. W. D. Bruno, and R. Droppa, Jr., J. Synchrotron Radiat. **13**, 46 (2006).
[34] G. H. Fecher *et al.*, J. Electron Spectrosc. Relat. Phenom. **156-158**, 97 (2007).
[35] F. Senf *et al.*, Nucl. Instrum. Methods Phys. Res. A **467-468**, 474 (2001).
[36] J. Tobola and J. Pierre, J. Alloys Compd. **296**, 243 (2000).
[37] K. Kroth, B. Balke, G. H. Fecher, V. Ksenofontov, C. Felser, and H.-J. Lin, Appl. Phys. Lett. **89**, 202509 (2006).
[38] I. Galanakis, P. H. Dederichs, and N. Papanikolaou, Phys. Rev. B **66**, 174429 (2002).
[39] G. H. Fecher, H. C. Kandpal, S. Wurmehl, and C. Felser, J. Appl. Phys. **99**, 08J106 (2006).
[40] Y. Stadnyk, V. Romaka, M. Shelyapina, Y. Gorelenko, L. Romaka, D. Furchart, A. Tkachuk, and V. Chekurin, J. Alloys Compd. **421**, 19 (2006).
[41] A. Sekiyama, T. Iwasaki, K. Matsuda, Y. Saitoh, Y. Onuki, and S. Suga, Nature (London) **403**, 396 (2000).
[42] G. Ertl and J. Küppers, *Low Energy Electrons and Surface Chemistry* (Chemie, Weinheim, 1985).
[43] D. Briggs and M. P. Seah, *Practical Surface Analysis by Auger and X-ray Photoelectron Spectroscopy* (Wiley, New York, 1983).
[44] J. J. Yeh and I. Lindau, At. Data Nucl. Data Tables **32**, 1 (1985).